Proceedings of NHTC'03
ASME Summer Heat Transfer Conference
Las Vegas, July 21-23, 2003

HT2003-47308

REDUCING CONVECTION EFFECTS IN SOLIDIFICATION BY APPLYING MAGNETIC FIELDS HAVING OPTIMIZED INTENSITY DISTRIBUTION

Marcelo J. Colaço[1]
Department of Mechanical Engineering, EE/COPPE
Federal University of Rio de Janeiro, UFRJ
Cid Universitaria, Cx. Postal 68503
Rio de Janeiro, RJ, 21945-970
BRAZIL
colaco@pobox.com

George S. Dulikravich[2]
Department of Mechanical and Aerospace Engineering
Multidisciplinary Analysis, Inverse Design & Optimization
(MAIDO) Institute, UTA Box 19018
The University of Texas at Arlington
Arlington, TX 76019, U.S.A.
dulikra@mae.uta.edu

Thomas J. Martin[3]
Pratt & Whitney Engine Company
Turbine Discipline Engineering & Optimization Group, M/S 169-20
400 Main Street, East Hartford, CT 06108, U.S.A.
thomas.martin@pw.utc.com

ABSTRACT

This paper presents a numerical procedure for achieving desired features of a melt undergoing solidification by applying an external magnetic field whose intensity and spatial distribution are obtained by the use of a hybrid optimization algorithm. The intensities of the magnets along the boundaries of the container are described as B-splines. The inverse problem is then formulated as to find the magnetic boundary conditions (the coefficients of the B-splines) in such a way that the gradients of temperature along the gravity direction are minimized. For this task, a hybrid optimization code was used that incorporates several of the most popular optimization modules; the Davidon-Fletcher-Powell (DFP) gradient method, a genetic algorithm (GA), the Nelder-Mead (NM) simplex method, quasi-Newton algorithm of Pshenichny-Danilin (LM), differential evolution (DE), and sequential quadratic programming (SQP).

Transient Navier-Stokes and Maxwell equations were discretized using finite volume method in a generalized curvilinear non-orthogonal coordinate system. For the phase change problems, an enthalpy formulation was used. The code was validated against analytical and numerical benchmark results with very good agreements in both cases.

[1] Postdoctoral Fellow. Lecturer.
[2] Professor and Director of MAIDO. Fellow of ASME.
[3] Systems Engineer. Member of ASME.

NOMENCLATURE

C_P	specific heat at constant pressure
B_x	magnetic flux component in x-direction
B_y	magnetic flux component in y-direction
g	acceleration of the gravity
Gr	Grashoff number
f	solid fraction
k	thermal conductivity
L	latent heat of solidification/melting
h	enthalpy
Ht	Hartmann number
n	partition coefficient in Scheil's equation (5)
P	pressure
Pr	Prandtl number
Ra	Rayleigh number
t	time
T	temperature
u	velocity component in x-direction
v	velocity component in y-direction
x, y	Cartesian coordinates

Greek letters

α	thermal diffusivity
β	thermal expansion coefficient
μ	fluid viscosity
μ_m	magnetic permeability

σ electric conductivity
ν kinematic viscosity

Subscripts
l liquid value
m melting value
s solid value
0 reference value

INTRODUCTION

During a controlled solidification process from a melt, it is important to understand the process of solid phase formation. The accumulated solid phase effectively reduces and deforms the cross sectional area of the passages and causes significant local variations in pressure and melt flow-field shear stresses. During the solidification process, melt flow is generated due to strong thermal buoyancy forces. This process cannot be effectively controlled in the case of strong heat transfer, except if influenced by a global body force. One such body force is the general electromagnetic Lorentz force that is created in any electrically conducting fluid when either a magnetic field or an electric field is applied.

We usually work with electrically conducting melts and liquid polymers where the resins are electrically conducting either because of the presence of iron atoms, salts, or acids. Thus, if an external magnetic field is applied, the molten resin flow-field will respond and the solid/liquid front shape and its speed could be manipulated non-intrusively [1-6].

The first objective of this work is to present some results obtained with a time-accurate code capable of simulating magnetohydrodynamic (MHD) flows with phase change.

The second objective is to combine this analysis code and an optimization code in order to minimize the natural convection effects in a cavity filled with a molten material. By minimizing the natural convection effects, it is possible to produce materials with less thermal stresses than those obtained in a presence of very strong buoyancy forces.

Two test cases are presented. The first involves only natural convection with a Rayleigh number equal to 10^5, while the second involves phase change in the presence of a natural convection with a Rayleigh number equal to 10^5. Applying an optimized magnetic field obtained by the use of a hybrid optimizer reduced the natural convection effects.

The difference between this and our previous work [7] is in the numerical method for dealing with the non-linear MHD model. The current method is able to use realistic values of physical properties, especially for the magnetic Prandtl number and is also time-accurate. The method was validated transient and steady state analytic solutions and then used it in a steady state magnetic field optimization study.

MAGNETOHYDRODYNAMIC (MHD) MODEL

The physical problem considered here involves the laminar magnetohydrodynamic natural convection of an incompressible Newtonian fluid. The fluid physical properties are assumed constant within each phase (solid or liquid) and linearly varying in the mushy region between the two phases. The energy source term resulting from viscous dissipation is neglected and buoyancy effects are approximated by the Boussinesq hypothesis. The modifications to the Navier-Stokes equations for the MHD fluid flow with heat transfer come from the electro-magnetic force on the fluid where all induced electric field terms have been neglected [3]. Then, the Navier-Stokes and the Maxwell equations can be written, for the Cartesian coordinate system as

$$\frac{\partial Q}{\partial t}+\frac{\partial E}{\partial x}+\frac{\partial F}{\partial y}=S \tag{1}$$

where

$$Q=\lambda\phi \tag{2.a}$$

$$E=\lambda u\phi^{*}-\Gamma\frac{\partial\phi^{***}}{\partial x} \tag{2.b}$$

$$F=\lambda v\phi^{**}-\Gamma\frac{\partial\phi^{***}}{\partial y} \tag{2.c}$$

The values of S, λ, ϕ, ϕ^{*}, ϕ^{**},ϕ^{***} and Γ are given in Table 1 for the equations of conservation of mass, x-momentum, y-momentum, energy, magnetic flux in the x-direction and magnetic flux in the y-direction.

Table 1. Parameters for the Navier-Stokes and Maxwell equations

Conservation of	λ	ϕ	ϕ^{*}	ϕ^{**}	ϕ^{***}	Γ	S
Mass	ρ	1	1	1	1	0	0
x-momentum	ρ	u	u	u	u	μ	$-\frac{\partial P}{\partial x}-\frac{B_y}{\mu_m}\left[\frac{\partial B_y}{\partial x}-\frac{\partial B_x}{\partial y}\right]$
y-momentum	ρ	v	v	v	v	μ	$-\frac{\partial P}{\partial y}-\rho g\left[1-\beta(T-T_0)\right]+\frac{B_y}{\mu_m}\left[\frac{\partial B_y}{\partial x}-\frac{\partial B_x}{\partial y}\right]$
Energy	ρ	h	h	h	T	K	$\frac{C_P}{\sigma\mu_m^2}\left[\frac{\partial B_y}{\partial x}-\frac{\partial B_x}{\partial y}\right]^2$
Magnetic flux in x-direction	1	B_x	0	B_x	B_x	$\frac{1}{\mu_m\sigma}$	$\frac{\partial(uB_y)}{\partial y}$
Magnetic flux in y-direction	1	B_y	B_y	0	B_y	$\frac{1}{\mu_m\sigma}$	$\frac{\partial(vB_x)}{\partial x}$

Note that we used the Boussinesq approximation for the variation of the density with temperature in the y-momentum conservation equation. Also note that in the energy conservation equation, the term $C_P T$ was replaced by the enthalpy, h, per unit mass. This is useful for problems dealing with phase change where we used the enthalpy method [8]. The above equations were transformed from the physical Cartesian (x,y) coordinates to the computational coordinate system (ξ,η) and solved by the finite volume method. The SIMPLEC method [9] was used to solve velocity-pressure coupling problem. The WUDS interpolation scheme [10] was used to obtain the values of u, v, h, B_x and B_y as well as their derivatives at the interfaces of each control volume. The resulting linear system was solved by the GMRES method.

PHASE CHANGE MODEL

In this paper we used the enthalpy method [8] to deal with the phase change problem. In this method, the energy equation appears as a mixed enthalpy-temperature equation. Thus, we must obtain some relationship between the temperature and the enthalpy to be used in the energy equation.

For the case of a binary alloy, if $h < h_{\text{solid}}$, we have

$$T = \frac{h}{C_{Ps}} \tag{3.a}$$

or, if $h > h_{\text{liquid}}$

$$T = \frac{h + T_s(C_{Pl} - C_{Ps}) - L}{C_{Pl}} \tag{3.b}$$

or yet, if $h_{\text{solid}} < h < h_{\text{liquid}}$

$$T = T_s = T_l = T_{melt} \tag{3.c}$$

For the case of mixture, we have a range of temperatures where the solidification might occur. Then, if $h_{\text{solid}} < h < h_{\text{liquid}}$,

$$T = \frac{h + [T_s(C_{Pl} - C_{Ps}) - L](1 - f)}{C_{Pl} + f(C_{Ps} - C_{Pl})} \tag{4}$$

where the solid fraction f is given by the Scheil's model [11]

$$f = 1 - \left(\frac{T_s - T}{T_s - T_l}\right)^{1/(n-1)} \tag{5}$$

In the above equation, we set the partition coefficient $n = 2$, which reduces the Scheil's model to the linear interpolation function. Note that if $T < T_{\text{solid}}$, f must be set to unity and, if $T > T_{\text{liquid}}$, f must be set to zero.

The magnetic and thermal properties were approximated as linear functions within the mushy region ($T_{\text{solid}} < T < T_{\text{liquid}}$) and kept constants within each phase. Thus, in the mushy region

$$\psi = f\psi_s + (1 - f)\psi_l \tag{6}$$

where ψ represents the density, thermal conductivity, viscosity, magnetic permeability and electric conductivity. For the viscosity of the solid phase we used

$$\frac{\mu_s}{\mu_l} \geq 10^6 \tag{7}$$

and for the specific heat at constant pressure within the mushy region, we used the thermodynamic property

$$C_P = \frac{\partial h}{\partial T} \approx \frac{\sqrt{\left(\frac{\partial h}{\partial x}\right)^2 + \left(\frac{\partial h}{\partial y}\right)^2}}{\sqrt{\left(\frac{\partial T}{\partial x}\right)^2 + \left(\frac{\partial T}{\partial y}\right)^2}} \tag{8}$$

Note that, if we are dealing with a mixture, the enthalpy is a function of the temperature, which is a function of the solid fraction which is itself a function of the temperature. Thus, if $h_{\text{solid}} < h < h_{\text{liquid}}$, we must solve a non-linear system for T. From Eqs. (4) and (5) we have

$$T - \frac{h + [T_s(C_{Pl} - C_{Ps}) - L]\left[\left(\frac{T_s - T}{T_s - T_l}\right)^{1/(n-1)}\right]}{C_{Pl} + \left[1 - \left(\frac{T_s - T}{T_s - T_l}\right)^{1/(n-1)}\right](C_{Ps} - C_{Pl})} = 0 \tag{9}$$

which can be solved for T by the secant method.

VALIDATION OF THE ANALYSIS CODE

The analysis code was validated against available analytical and experimental benchmark results. For problems without phase change and without magnetic fields, other validations can be found [12, 13]. Given below are presentations of the validations for phase change problems and for problems with magnetic fields.

Pouiseuille-Hartmann Flow

The Pouiseuille-Hartmann flow is a one-dimensional flow of an electrically conducting, incompressible, viscous fluid between two stationary infinite parallel plates with a uniform external magnetic field applied orthogonal to the plates.

Let us consider the following geometry, where the fluid enters the domain at $x = 0$ and the uniform magnetic field is applied orthogonal to the walls located at $y = 0$ and $y = 2H$.

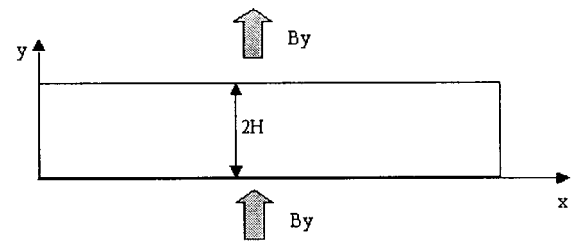

Figure 1. Geometry for the Poiseuille-Hartmann flow.

The analytical solution for the velocity field is given as [14]

$$u(y) = \frac{dP}{dx}\frac{H^2}{\mu}\left[\frac{\cosh(Ht) - \cosh\left(Ht\frac{y}{H}\right)}{Ht\sinh(Ht)}\right] \tag{10}$$

where the Hartmann number is defined as:

$$Ht = B_0 H_0 \sqrt{\frac{\sigma}{\mu}} \tag{11}$$

Let us consider the following properties for silicon:

$\rho = 2550$ kg m^{-2} $\quad C_P = 1059$ J kg^{-1} K^{-1}
$K = 64$ W m^{-1} K^{-1} $\quad \mu = 7.018\text{x}10^{-4}$ kg m^{-1} s^{-1}
$\sigma = 12.3\text{x}10^{5}$ Ω^{-1} m^{-1} $\quad \beta = 1.4\text{x}10^{-4}$ K^{-1}
$\mu_m = 1.2566\text{x}10^{-5}$ T m A^{-1}

By choosing the channel half-width as $H_0 = 0.1$ m, we have evaluated the accuracy of the MHD code against the following three test cases

Test case no.	Ht	B_0 (T)
1	1.0	$2.3887\text{x}10^{-4}$
2	5.0	$1.1943\text{x}10^{-3}$
3	10.0	$2.3887\text{x}10^{-3}$

The following figures show the comparison between the numerically obtained and the analytical results for a non-uniform grid with 80x80 cells clustered symmetrically towards the walls. One can note that the analytical and numerical results have an excellent agreement, with an error less than one percent close to the walls and less than 0.05 percent at the center of the channel. It is worth noticing that, as the Ht number was increased, the velocity profile became more flat.

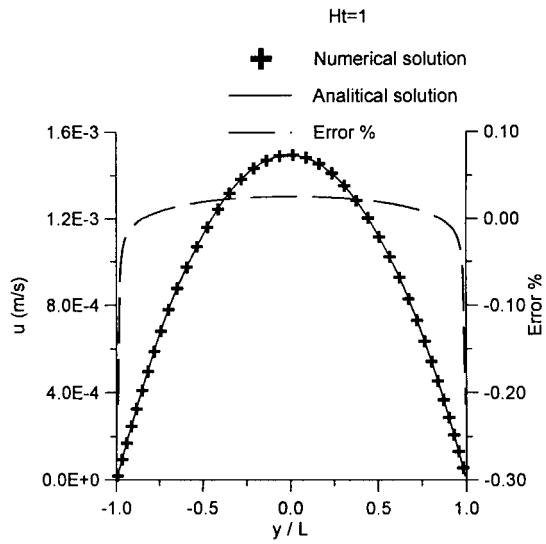

Figure 2. Test case no. 1 for the Poiseuille-Hartmann flow.

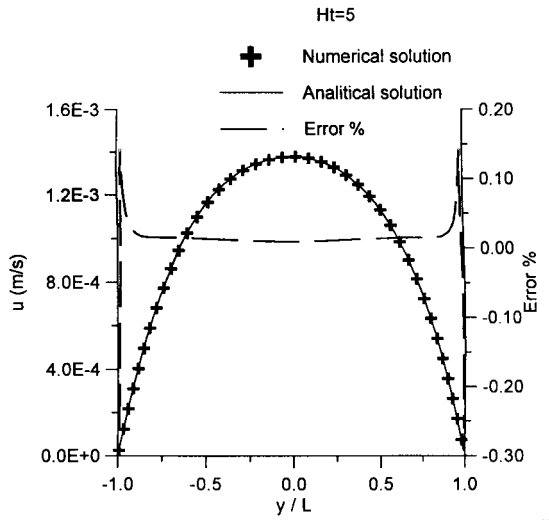

Figure 3. Test case no. 2 for the Poiseuille-Hartmann flow.

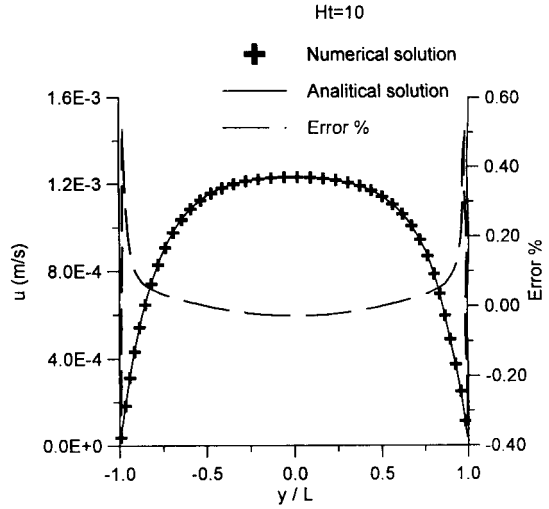

Figure 4. Test case no. 3 for the Poiseuille-Hartmann flow.

Solidification/Melting in a Heat Conduction Problem

Let us consider the following one-dimensional heat conduction problem with phase change in a semi-infinite medium, where the coordinate $x = 0$ is kept at a temperature $T_0 < T_m$ and the infinity $x \to \infty$ is kept at $T_i > T_m$. The temperatures within each phase T_s and T_l varies with the position x and with the time t. The interface between the two phases vary its position with time as a function $s(t)$.

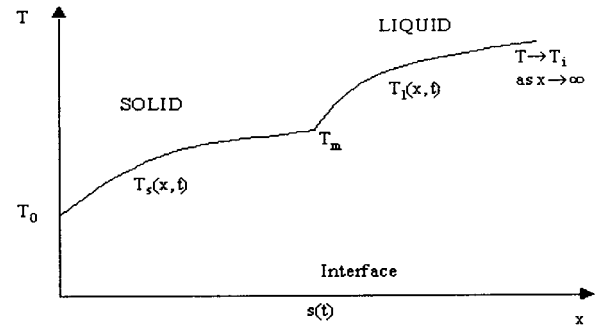

Figure 5. Phase change in a semi-infinite medium.

The mathematical formulation of this problem for the solid phase is given as

$$\frac{\partial^2 T_s}{\partial x^2} = \frac{1}{\alpha_s}\frac{\partial T_s(x,t)}{\partial t} \quad \text{in } 0 < x < s(t),\ t > 0 \tag{12.a}$$

$$T_s(x,t) = T_0 \quad \text{at } x = 0,\ t > 0 \tag{12.b}$$

and for the liquid phase as

$$\frac{\partial^2 T_l}{\partial x^2} = \frac{1}{\alpha_l}\frac{\partial T_l(x,t)}{\partial t} \quad \text{in } s(t) < x < \infty,\ t > 0 \tag{13.a}$$

$$T_l(x,t) = T_i \quad \text{as } x \to \infty,\ t > 0 \tag{13.b}$$

$$T_l(x,t) = T_0 \quad \text{for } t = 0,\ x > 0 \tag{13.c}$$

The coupling conditions at the interface $x = s(t)$ are

$$T_s(x,t) = T_l(x,t) = T_m \quad \text{at } x = s(t),\ t > 0 \tag{14.a}$$

$$k_s\frac{\partial T_s}{\partial x} - k_l\frac{\partial T_l}{\partial x} = \rho L\frac{ds(t)}{dt} \quad \text{at } x = s(t),\ t > 0 \tag{14.b}$$

The analytical solution is given as [15]

$$T_s(x,t) = (T_m - T_0)\frac{erf\left[x/(2\alpha_s t)^{1/2}\right]}{erf(\lambda)} + T_0 \tag{15.a}$$

$$T_l(x,t) = (T_m - T_i)\frac{erfc\left[x/(2\alpha_l t)^{1/2}\right]}{erf\left[\lambda(\alpha_s/\alpha_l)^{1/2}\right]} + T_i \tag{15.b}$$

where λ is given as a transcendental expression by

$$\frac{e^{-\lambda^2}}{erf(\lambda)} + \frac{k_l}{k_s}\left(\frac{\alpha_l}{\alpha_s}\right)^{1/2}\frac{T_m - T_i}{T_m - T_0}\frac{e^{-\lambda^2(\alpha_s/\alpha_l)}}{erfc\left[\lambda(\alpha_s/\alpha_l)^{1/2}\right]} = \frac{\lambda L\sqrt{\pi}}{C_{Ps}(T_m - T_0)} \tag{16}$$

The solid-liquid interface location $s(t)$ is given by

$$s(t) = 2\lambda(\alpha_s t)^{1/2} \tag{17}$$

where α is the thermal diffusivity defined as

$$\alpha = \frac{k}{\rho C_P} \tag{18}$$

The one-dimensional heat conduction problem with phase change was approximated as a two-dimensional plate where the top and bottom surfaces were kept insulated in order to reduce the problem from the two-dimensional to the one-dimensional case.

The right boundary condition, located at x = 3.0 m, was considered to be at the "infinity" and kept at T_i = 1688.0 K. The left boundary condition was equal to the initial boundary condition T_0 = 1676.0 K. The melting temperature was T_m = 1683.0 K.

For this problem, we used silicon with the following properties

k_l = 64 W m^{-1} K^{-1}	k_s = 22 W m^{-1} K^{-1}
ρ = constant = 2550 kg m^{-3}	L = 1.803 x 10^6 J kg^{-1}
C_{Pl} = 1059 J kg^{-1} K^{-1}	C_{Ps} = 1038 J kg^{-1} K^{-1}

The following figures 6-9 show the comparisons between the numerically obtained and the analytical results at three different times, where the temperature is plotted as a function of the distance x. The point where the curve changes its slope represents the place where the solid-liquid interface is located.

One can see the excellent agreement between the solutions, showing the good accuracy of the method for transient heat conduction problems with phase change. It is interesting to note that, as the interface moves towards the right boundary the current results start slightly deviating from the analytical ones in the region close to the right boundary (Figures 8 and 9). This is due to the fact that we are approximating the infinity with a finite value of x at the right end of the plate.

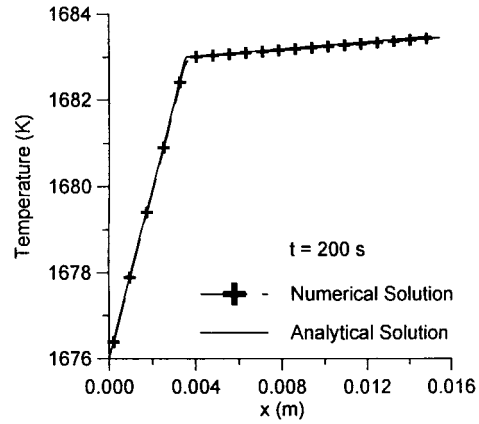

Figure 6. Heat conduction phase change problem (t = 200 s).

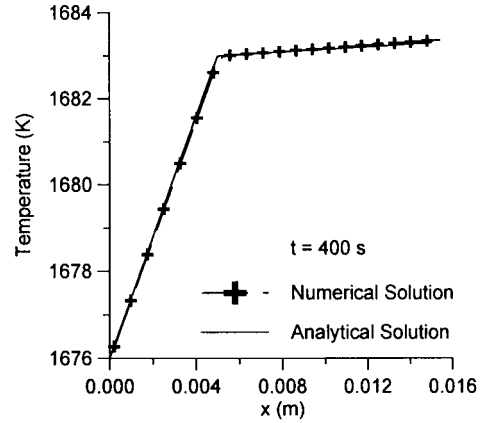

Figure 7. Heat conduction phase change problem (t = 400 s).

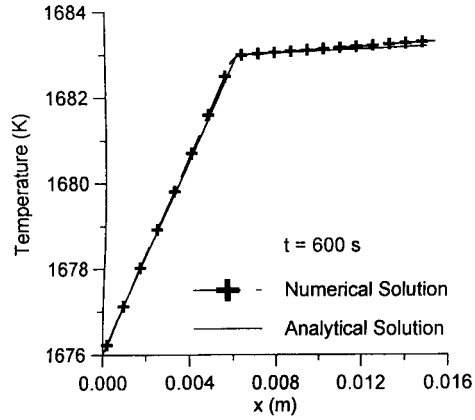

Figure 8. Heat conduction phase change problem (t = 600 s).

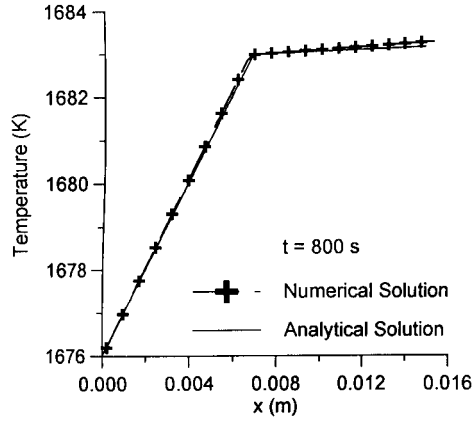

Figure 9. Heat conduction phase change problem (t = 800 s).

Solidification/Melting in a Heat Convection Problem

In order to validate the transient solidification simulation code in a problem involving natural convection, we compared the present code with the results published by Bertrand et al. [16]. They presented several methods published by other researchers for solving the same problem and compared those numerical solutions with their own solutions. The problem presented by Bertrand et al. was a square cavity, filled with a solid material whose initial temperature T_0 was set equal to the melting temperature T_m, as shown in the Figure 10.

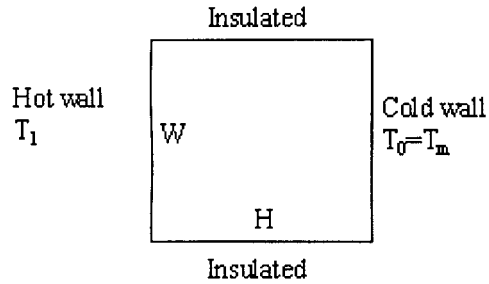

Figure 10. Geometry for the heat convection problem.

The natural convection initiates when the left wall is exposed to a temperature greater than the melting temperature. Then, the material starts to melt and the natural convection initiates at the left boundary. The top and bottom walls were kept insulated.

The physical properties, taken from the Bertrand et al. paper, are

$K = 60$ W m K^{-1}	$C_P = 200$ J kg K^{-1}
$\rho = 7500$ kg m^{-3}	$\alpha = 4\text{x}10^{-5}$ m^2 s^{-1}
$\nu = 8\text{x}10^{-7}$ m^2 s^{-1}	L = 6x10^4 J kg^{-1}
$T_m = 232$ °C	$\Delta T = 3$ °C
$\beta = 8.3$ x 10^{-4} K^{-1}	$H = W = 0.10$ m
$g = 10$ m s^{-2}	

The following figures 11-14 show the comparisons between the present results and those presented by Bertrand et al. for a grid with 90x90 cells at t = 100 s, 250 s, 1000 s and 2500 s. In each figure, the position of the solidification front is plotted within the cavity, whose dimensions are normalized by the length, H. In Bertrand's paper, several solutions, from different methods were presented corresponding to each of the curves shown.

One can note a good agreement between the present results and Bertrand's solutions. Note that the solutions are all located in a range and the present results are located within this range.

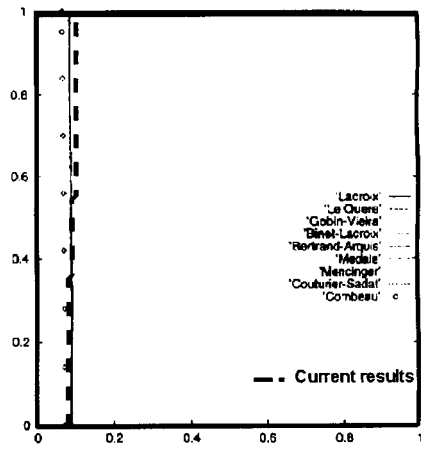

Figure 11. Heat convection phase change problem (t = 100 s).

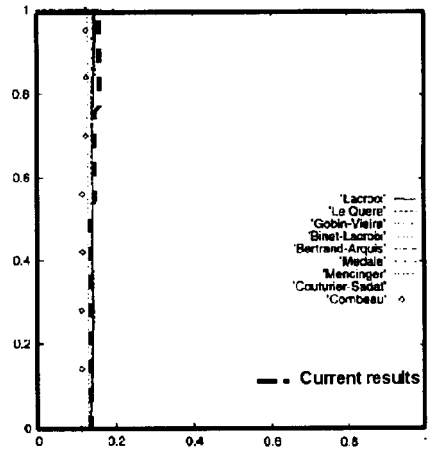

Figure 12. Heat convection phase change problem (t = 250 s).

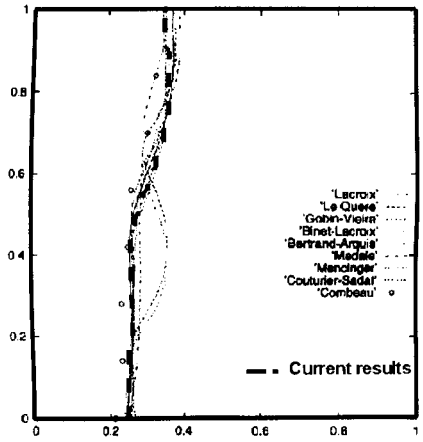

Figure 13. Heat convection phase change problem (t = 1000 s).

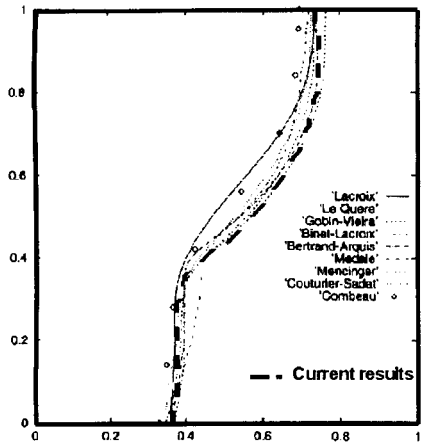

Figure 14. Heat convection phase change problem (t = 2500 s).

MHD Problem with Natural Convection

In order to validate the MHD problem in a presence of natural convection we compared the present results with numerical results obtained by Ozoe and Okada [17]. In this problem the flow is driven by two kinds of body forces: one due to thermal buoyancy in the y-momentum conservation equation and the other due to the presence of the magnetic fields.

The problem considered by Ozoe and Okada was a cubical cavity whose transverse section is shown in the Figure 15.

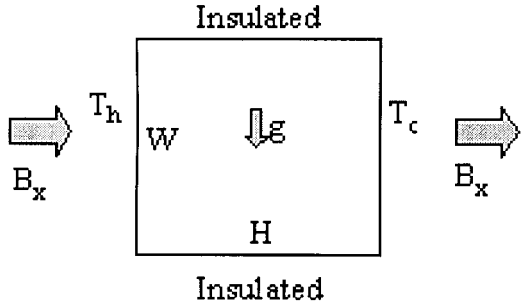

Figure 15. Geometry for the MHD problem.

Ozoe and Okada used the following parameters for silicon: Pr = 0.054, Ra = 10^6, Ht = 0, 300, 500 where the Hartmann (Ht) number was given by Eq. (11) and the Prandtl (Pr), Rayleigh (Ra) and Grashoff (Gr) numbers are given as

$$\mathrm{Pr} = \frac{\mu}{\rho\alpha} \qquad Ra = Gr\,\mathrm{Pr} \qquad Gr = \frac{g\beta(T_h - T_c)W^3}{\nu^2} \qquad \text{(19.a-c)}$$

The physical properties for silicon are the same as previously defined, except for viscosity, which, using the above parameters is obtained as μ = 0.00326346 kg m^{-1} s^{-1}. Choosing W = 0.15 m and g = 9.81 m s^{-2}, we obtain ΔT = 6.54351 K. Then, for the various Ht numbers, we obtained

$Ht = 0$ $\quad B_0 = 0.0$ T
$Ht = 300$ $\quad B_0 = 0.103019$ T
$Ht = 500$ $\quad B_0 = 0.171698$ T

Figures 16-18 show the comparisons between the present results and those obtained by Ozoe and Okada. The figures show the isotherms obtained in the presence of magnetic fields with Hartmann numbers equal to 0, 300 and 500. Note that, for Ht = 0, the problem reduces to the natural convection problem without any magnetic field applied. In Ozoe and Okada's paper, the solutions were obtained with a grid size of 21x15 cells, while the current results were obtained with a grid size of 60x60 cells. One can notice that the results have a reasonable agreement. It is also interesting to note that as we increase the Ht number, the natural convection effects are gradually reduced.

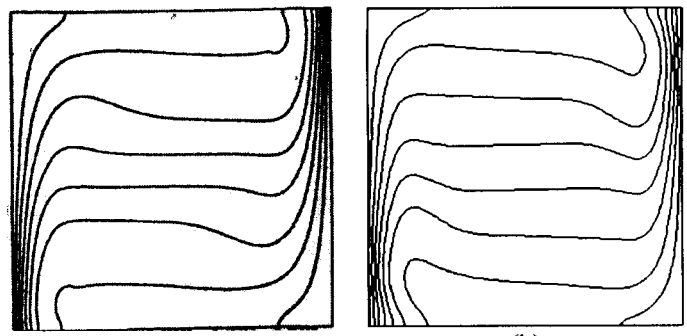

(a) (b)

Figure 16. Ozoe and Okada's (a) and current (b) results (Ht = 0)

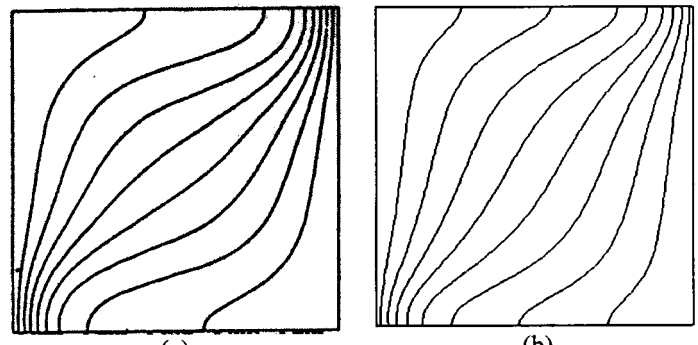

(a) (b)

Figure 17. Ozoe and Okada's (a) and current (b) results (Ht = 300).

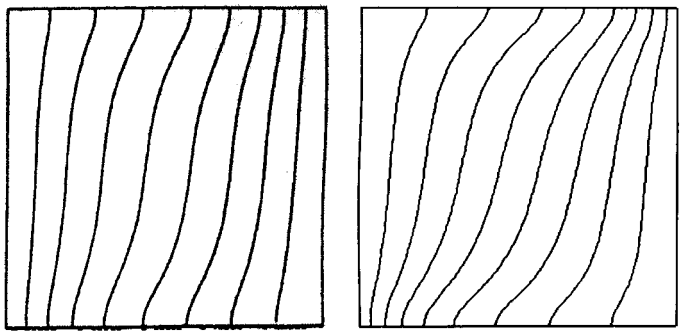

(a) (b)

Figure 18. Ozoe and Okada' (a) and current (b) results ($Ht = 500$).

INVERSE PROBLEM OF DETERMINING THE UNKNOWN MAGNETIC FIELD BOUNDARY CONDITIONS

In this paper we deal with the inverse determination of the magnetic boundary conditions that give some pre-specified flow-field within some region [7, 18, 19]. Figure 19 shows the geometry and the boundary conditions for the test cases considered here.

The height and length of the cavity were equal to 0.15 m. The top and bottom walls were kept thermally insulated. The left boundary was kept at a "hot" temperature while the right wall was kept at a "cold" temperature. For the first test case, there was no phase change, since the "hot" and "cold" temperatures were above the melting temperature.

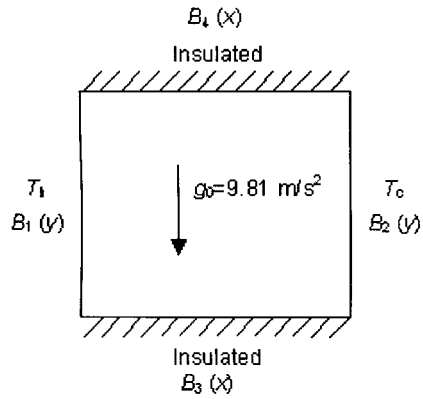

Figure 19. Geometry and boundary conditions.

The four walls were subjected to unknown magnetic field distributions whose directions were made orthogonal to each wall. In order to satisfy the magnetic flux conservation equation

$$\nabla \bullet \mathbf{B} = 0 \tag{20}$$

the following periodic conditions were imposed

$$B_1(y) = B_2(y) \tag{21.a}$$
$$B_3(x) = B_4(x) \tag{21.b}$$

The objective was to minimize [20] the natural convection effects by reducing the gradient of temperature along the y direction, thus trying to obtain a temperature profile similar to those obtained for pure conduction. The objective function to be minimized is then formulated as [7]

$$F = \sqrt{\frac{1}{\#cells}\sum_{i=1}^{\#cells}\left(\frac{\partial T_i}{\partial y_i}\right)^2} \tag{22}$$

The magnetic field boundary conditions were inversely determined at either four or six points equally spaced for each of the four boundaries and interpolated using B-splines for the other points at those boundaries. The magnetic boundary conditions at x = 0.15 m and y = 0.15 m were then obtained using periodic conditions from Eqs. (21.a) and (21.b).

The physical properties were the same as previously used for the comparison with the Ozoe and Okada's paper. For the first test case, the temperature difference T_h-T_c was set equal to 0.654351 K, which gives a Rayleigh number of 10^5.

Figure 20 shows the velocity and temperature profiles predicted for the first test case without any magnetic flux applied and no phase change. Figure 21 shows the optimized velocity and temperature profile using four points on each boundary for the estimation of the magnetic boundary conditions. One can see that the gradients of temperature in the y direction are reduced. Figure 22 shows the optimized boundary conditions for x = 0 and y = 0 and Figure 23 shows the convergence history of the process. One can see that the differential evolution (DE) algorithm did almost all the work.

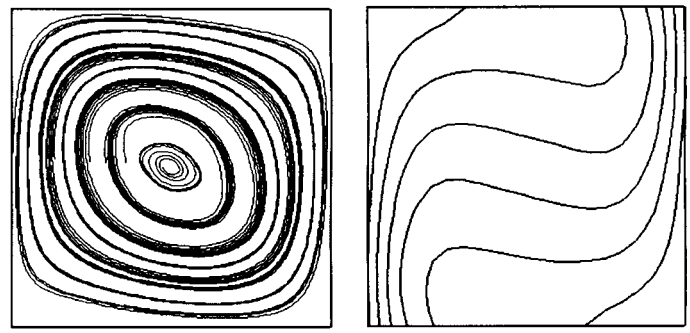

(a) (b)

Figure 20. Streamlines (a) and isotherms (b) with **B** = 0.

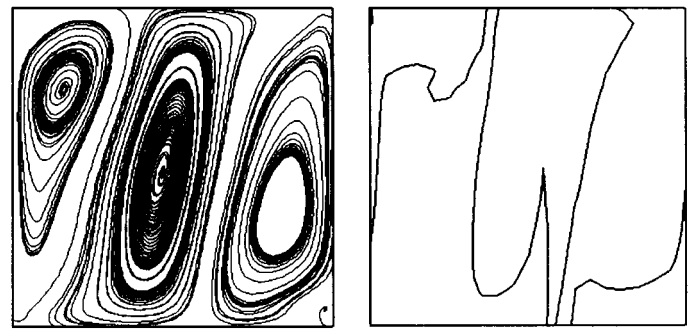

(a) (b)

Figure 21. Streamlines (a) and isotherms (b) resulting from **B** optimized at four points per boundary.

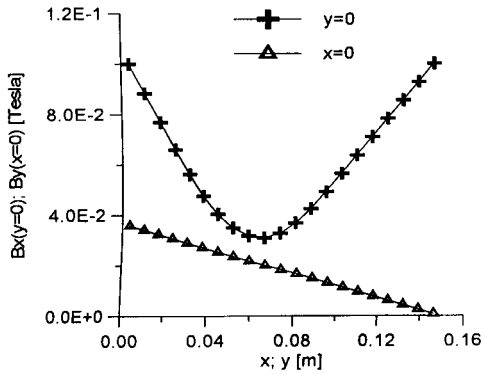

Figure 22. Optimized magnetic boundary conditions at $x = 0$ and $y = 0$ with the estimation of **B** at four points per boundary.

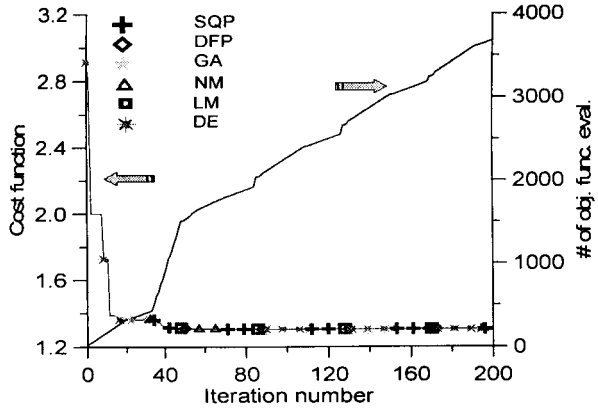

Figure 23. Optimization convergence history for the estimation of **B** at four points per boundary.

Figure 24 shows the velocity and temperature profiles resulting from six optimized terms in the B-spline on each boundary for the estimation of the magnetic boundary conditions. Using more design variables (B-spline control points) in the optimization creates better results where the gradients of temperature in the y direction are further reduced.

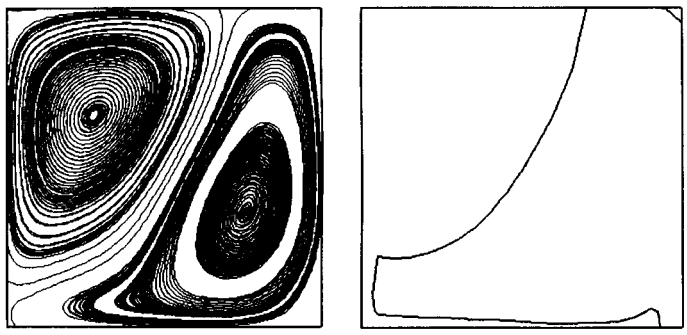

(a) (b)

Figure 24. Streamlines (a) and isotherms (b) resulting from **B** optimized at six points per boundary.

Figure 25 shows the optimized boundary condition for $x = 0$ and $y = 0$ and Figure 26 shows the convergence history of the process where one can see that the differential evolution (DE) and genetic algorithm (GA) modules did almost all the work.

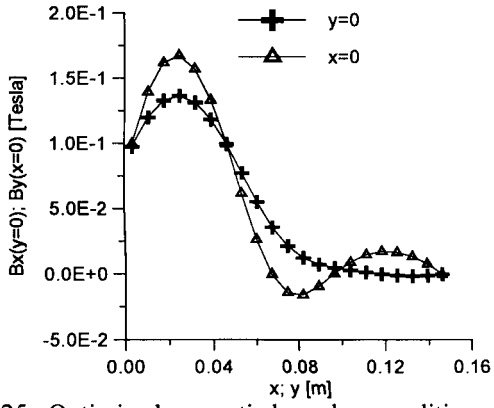

Figure 25. Optimized magnetic boundary conditions at $x = 0$ and $y = 0$ with the estimation of **B** at six points per boundary.

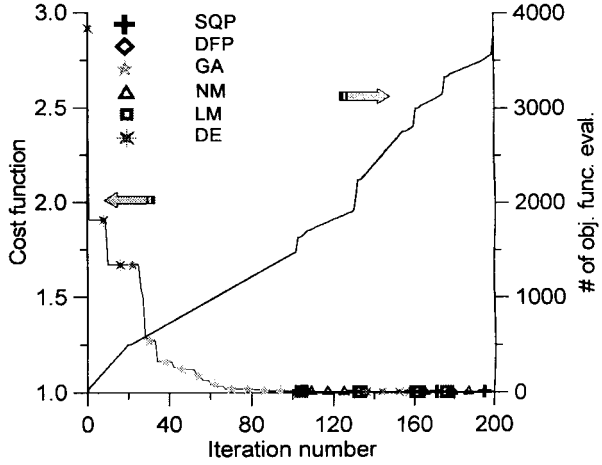

Figure 26. Optimization convergence history for the estimation of **B** at six points per boundary.

As a second test case, let us try to minimize the curvature of the isotherms in a solidifying process after a pre-specified time from the start of the solidifying process. The following physical properties were used.

$\rho_l = 2550$ kg m^{-3}	$\rho_l = 2330$ kg m^{-3}
$k_l = 64$ W m^{-1} K^{-1}	$k_s = 22$ W m^{-1} K^{-1}
$C_{Pl} = 1059$ J kg^{-1} K^{-1}	$C_{Ps} = 1038$ J kg^{-1} K^{-1}
$\mu_l = 0.0032634$ kg m^{-1} s^{-1}	$\mu_s = 1.0 \times 10^3$ kg m^{-1} s^{-1}
$\sigma_l = 12.3 \times 10^5$ 1/m Ω	$\sigma_s = 4.3 \times 10^4$ 1/m Ω
$\beta = 8.3 \times 10^{-4}$ K^{-1}	$g = 9.81$ m s^{-2}
$\mu_m = 1.2566 \times 10^{-5}$ T m A^{-1}	$L = 1.803 \times 10^6$ J kg^{-1}

The temperature difference T_h-T_c was set equal to 6.54351 K (T_h = 1686.04351 K, T_c = 1676.5 K) and the length of the square container was taken as 0.069624 m, which gives a Rayleigh number of 10^5. The solid and liquid temperatures were equal to 1681.0 K and 1686.0 K, respectively. Thus, a mushy region exists between the phases.

The initial condition was set as $T_0 = T_h$. Then, the solidifying process starts at the right wall, where $T = T_c$.

Figure 27 shows the streamlines and isotherms for this test case, predicted at 500 seconds.

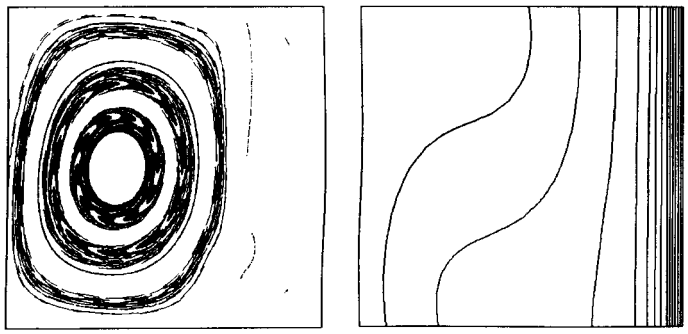

(a) (b)

Figure 27. Streamlines (a) and isotherms (b) at 500 s with **B**=0.

Figure 28 shows the streamlines and isotherms resulting from optimization of six B-spline points for the estimation of the magnetic boundary conditions on each boundary. The boundary conditions at the other points were interpolated using B-splines. One can see that the curvature of the isotherms is smaller than in the Figure 27.

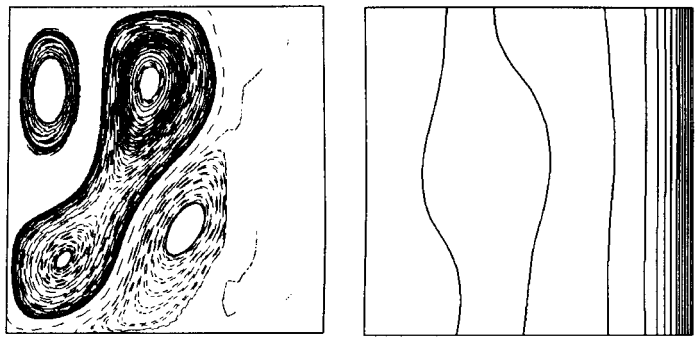

(a) (b)

Figure 28. Streamlines (a) and isotherms (b) at 500 s resulting from the optimization of **B** at six points per boundary.

Figure 29 shows the optimized boundary condition for x = 0 and y = 0. Figure 30 shows the convergence history of the optimization process where one can see that the genetic algorithm (GA) module did almost all the work. The iterative process was forced to stop after 70 iterations due to the high computational cost involved.

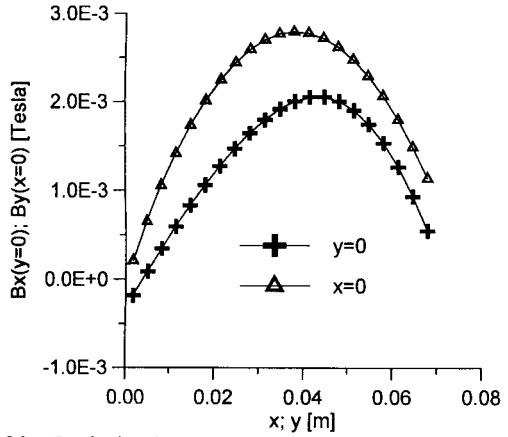

Figure 29. Optimized magnetic boundary conditions at 500 s with the estimation of **B** at six points per boundary.

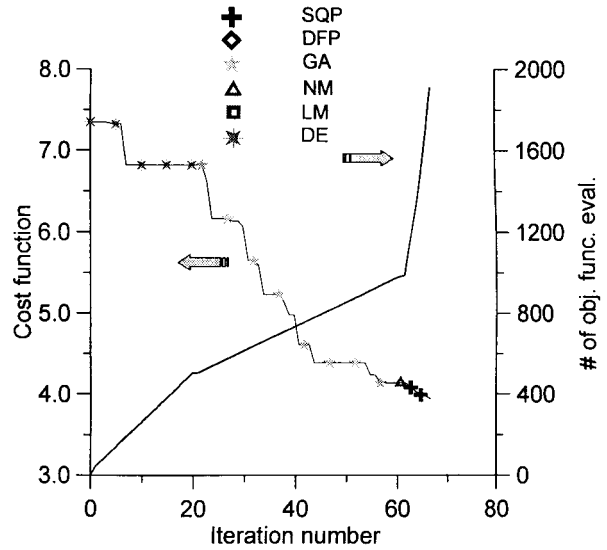

Figure 30. Optimization convergence history for the estimation of **B** at six points per boundary at 500 s.

CONCLUSIONS

In this paper we showed the results of a time-accurate MHD code that is capable of dealing with phase change problems. The code was validated against analytical and numerical (benchmark) results showing excellent agreement and was applied to test cases involving steady state optimization. The ability to minimize the natural convection effects in problems with and without phase change was demonstrated by utilizing an optimized distribution of magnetic filed along the boundaries of a container. A hybrid constrained optimization algorithm was used in reducing the isotherms pattern to those similar to pure conduction problems.

AKNOWLEDGEMENTS

The first author is grateful for the postdoctoral fellowship received from University of Texas at Arlington and from CNPq, a Brazilian council for scientific and technological development.

The second author is grateful for the partial support provided for this research on the grant NSF DMS-0073698 administered through the Computational Mathematics program.

REFERENCES

1. Motakeff, S., 1990, "Magnetic Field Elimination of Convective Interference With Segregation During Vertical-Bridgman Growth of Doped Semiconductors", *Journal of Crystal Growth*, vol. 104, pp. 833-850.
2. Dulikravich, G. S., Ahuja, V. and Lee, S., 1994, "Modeling Three-Dimensional Solidification With Magnetic Fields and Reduced Gravity", *International Journal of Heat and Mass Transfer*, vol. 37, no. 5, pp. 837-853.
3. Dulikravich, G. S., 1999, "Electro-Magneto-Hydrodynamics and Solidification," Chapter no. 9 in *Advances in Flow and Rheology of Non-Newtonian Fluids*, Part B (eds. D.A. Siginer, D. De Kee and R.P. Chhabra), Rheology Series, 8, Elsevier Publishers, pp. 677-716.
4. Fedoseyev, K. I., Kansa, E. J., Marin, C. and Ostrogorsky, A. G., 2001, "Magnetic Field Suppression of

Semiconductor Melt Flow in Crystal Growth: Comparison of Three Methods for Numerical Modeling", *Japanese CFD Journal*, vol. 9, pp. 325 - 333.

5. Dennis, B. H. and Dulikravich, G. S., 2000, "Simulation of Magnetohydrodynamics With Conjugate Heat Transfer", *Proceedings of ECCOMAS2000 - European Congress on Computational Methods in Applied Sciences and Engineering* (eds. E. Onate, G. Bugeda and B. Suarez), Barcelona, Spain, September 11-14, 2000.
6. Dennis, B. H. and Dulikravich, G. S., 2002, "Magnetic Field Suppression of Melt Flow in Crystal Growth", *International Journal of Heat & Fluid Flow*, vol. 23, no. 3, pp. 269-277.
7. Dulikravich, G. S., Colaço, M. J., Martin, T. J. and Lee, S., 2003, "Optimization of Intensities, and Orientations of Magnets Controlling Melt Flow During Solidification", *J. of Materials and Manufacturing Processes*, to appear.
8. Voller, V. R., Brent, A. D. and Prakash, C., 1989, "The Modeling of Heat, Mass and Solute Transport in Solidification Systems", *Int. J. Heat Mass Transfer*, vol. 32, pp. 1719-1731.
9. Van Doormal, J. P. and Raithby, G. D., 1984, "Enhancements of the SIMPLE Method for Predicting Incompressible Fluid Flow", *Numerical Heat Transfer*, vol. 7, pp. 147-163.
10. Raithby, G. D. and Torrance, K. E., 1974, "Upstream-Weighted Differencing Schemes and Their Application to Elliptic Problems Involving Fluid Flow", *Computers & Fluids*, vol. 2, pp. 191-206.
11. Rappaz, M., 1989, "Modelling of Microstructure Formation in Solidification Proccess", *International Materials Reviews*, vol. 34, no. 3, pp. 93-123.
12. Colaço, M. J. and Orlande, H. R. B., 2001, "Inverse Forced Convection Problem of Simultaneous Estimation of Two Boundary Heat Fluxes in Irregularly Shaped Channels", *Numerical Heat Transfer – Part A*, vol. 39, pp. 737-760.
13. Colaço, M. J. and Orlande, H. R. B., 2002, "Inverse Convection Problems in Irregular Geometries", *Proc. of the 21st Southeastern Conference on Theoretical and Applied Mechanics*, Orlando, FL, 2002.
14. Woodson, H. H. and Melcher, J. R., 1968, *Electromechanical Dynamics – Part III: Elastic and Fluid Media*, John Wiley & Sons, Inc., New York.
15. Özisik, M. N., 1993, *Heat Conduction*, Wiley-Interscience, 2nd edition.
16. Bertrand, O., Binet, B., Combeau, H., Couturier, S., Delannoy, Y., Gobin, D., Lacroix, M., Le Quéré, P., Médale, M., Mencinger, J., Sadat, H. and Vieira, G., 1999, "Melting Driven by Natural Convection – A Comparison Exercise: First Results", *Int. J. Therm. Sci.*, vol. 38, pp. 5-26.
17. Ozoe, H. and Okada, K., 1989, "The Effect of the Direction of the External Magnetic Field on the Three-Dimensional Natural Convection in a Cubical Enclosure", *Int. J. Heat Mass Transfer*, vol. 32, no. 10, pp. 1939-1954.
18. Dennis, B. H. and Dulikravich, G. S., 2001, "Optimization of Magneto-Hydrodynamic Control of Diffuser Flows Using Micro-Genetic Algorithm and Least Squares Finite Elements", *Journal of Finite Elements in Analysis and Design*, vol. 37, no. 5, pp. 349-363.
19. Dulikravich, G. S., Colaco, M., Martin, T. J. and Lee, S., 2003, "Magnetized Fiber Orientation and Concentration Control in Solidifying Composites", *Journal of Composite Materials*, to appear.
20. Dulikravich, G. S., Martin, T. J., Dennis, B. H. and Foster, N. F., 1999, "Multidisciplinary Hybrid Constrained GA Optimization", Chapter 12 in *EUROGEN'99 - Evolutionary Algorithms in Engineering and Computer Science: Recent Advances and Industrial Applications* (eds. K. Miettinen, M. M. Makela, P. Neittaanmaki and J. Periaux), John Wiley & Sons, Jyvaskyla, Finland, May 30 - June 3, 1999, pp. 233-259.